Calibration for IR absorbance measurements of OH in apatite

Karen L. Wang,[1] Youxue Zhang,[1,*] and Fabian U. Naab[2]

[1]Department of Geological Sciences, University of Michigan, Ann Arbor, Michigan 48109, U.S.A.
[2]Department of Nuclear Engineering and Radiological Sciences, University of Michigan, Ann Arbor, Michigan 48109, U.S.A.
* corresponding author, email: youxue@umich.edu

ABSTRACT

In this work, we have calibrated the infrared (IR) method for determining OH concentration in apatite with absolute concentrations obtained through elastic recoil detection (ERD) analysis. IR spectra were collected on oriented, single-crystal apatite samples using polarized transmission infrared spectroscopy. The weight percent H_2O is 0.001199 ± 0.000029 (the error is given at 1σ level hereafter) times A/d, where A is the linear absorbance peak height measured using polarized IR when the light vector **E** is parallel to the **c**-axis of the apatite crystal, and d is the sample thickness in cm. This corresponds to a linear molar absorptivity, $\varepsilon = 470 \pm 11$ L mol^{-1} cm^{-1}. The calibration using linear absorbance can be applied when there is only one dominant peak at 3540 cm^{-1}. If other peaks are significant, then the integrated molar absorptivity, $\varepsilon = (2.31 \pm 0.06) \times 10^4$ L mol^{-1} cm^{-2}, should be used. The detection limit of H_2O concentration in apatite by IR approaches ppm level for wafers of 0.1 mm thickness. The accuracy based on our calibration is 5-10% relative.

Keywords: apatite, water concentration, IR spectroscopy, ERD analysis

INTRODUCTION

Apatite is a common accessory mineral in igneous rocks on Earth, Moon (e.g., Boyce et al. 2010; McCubbin et al. 2010), and Mars (e.g., McCubbin and Nekvasil 2008). Its general formula is often written as $M_5(ZO_4)_3X$, where the M-site holds large cations such as Ca^{+2}, Sr^{+2}, and Pb^{+2}, the Z-site is usually occupied by P but can also hold As, Si, C, or S (with appropriate charge balance substitutions), and the X-site is most commonly filled by F, Cl, and OH. The amounts of F, Cl, and OH in apatite can indicate fluid conditions during crystal formation (e.g., Mathez and Webster 2005; Boyce and Hervig 2009; Webster et al. 2009). Specifically, OH in igneous apatite can be a measure of water concentration (e.g., Boyce et al. 2010). Previously, OH concentration in apatite (typically expressed as H_2O wt% or ppm) has been estimated by combining electron microprobe analyses of F and Cl with knowledge of mineral stoichiometry (e.g., Mathez and Webster 2005; McCubbin and Nekvasil 2008). However, the X-ray intensity for the F Kα peaks when analyzing apatite varies as a function of electron beam exposure time and crystallographic orientation (Stormer et al. 1993; Henderson et al. 2010), which also adversely affects the detection limit of OH. Recently, SIMS has also been applied to measure H_2O content in apatite (Boyce et al. 2010; McCubbin et al. 2010).

Fourier transform infrared spectroscopy (FTIR) can detect the OH fundamental stretching peaks in apatite at ~3540 cm^{-1} (e.g., Bhatnaga 1967; Levitt and Condrate Sr. 1970; Tacker 2004) with potentially high spatial resolution (routinely 50 μm x 50 μm with a microscope attachment, and possibly 20 μm x 20 μm) and high sensitivity. However, the absorbance bands only indicate the relative concentration of OH. In order to determine absolute OH concentration, a calibration of the IR method using an independent method for determining absolute concentration is needed. One method for determining the absolute water concentration is extraction of H_2O (e.g., Nadeau

et al. 1999). This method requires picking a large quantity of inclusion-free apatite fragments, which is often prohibitively difficult. Another method is elastic recoil detection (ERD) (e.g., Aubaud et al. 2009; Bureau et al. 2009; Cherniak et al. 2010), a surface method that can determine absolute H concentration in a surface layer of about 400 nm, but requires large sample size (> 4 mm diameter, at the University of Michigan Ion Beam Laboratory). That is, the ERD method cannot be applied to analyze small apatite crystals, such as those found as accessory minerals in typical igneous rocks.

In this work, we present a calibration for absorbance measurements of OH by analyzing large, gem-quality, apatite crystals using both FTIR and ERD. With the calibration, absolute water concentration of small apatite crystals can be determined to high accuracy using polarized FTIR.

SAMPLES AND ANALYTICAL METHODS

Samples

Five large, gem-quality, single-crystal apatite samples were obtained from a variety of localities: Durango, Mexico (two crystals labeled DurMex and Cerro); High Atlas Mountains, Morocco (HAM); and two crystals of unknown locality purchased from an online vendor (Gem3 and Gem4). All were light yellow green and transparent before polishing. A large crystal from Silver Crater Mine which was not of gem quality was also analyzed, but the results are not used (see discussion below).

DurMex was originally ~6 mm in diameter and ~15 mm long, with visible vapor phase inclusions. When viewed under a microscope at 10x magnification, the inclusions appeared to be in linear strings (possibly the result of planar healed fractures). These areas were avoided during FTIR analysis. Due to their placement, we were unable to avoid the inclusions during ERD

analysis. However, because of their small size, and the low penetration depth (400 nm) of the ion beam, we do not think the ERD analysis was affected by the presence of the inclusions.

Cerro was originally ~15 mm in diameter and ~18 mm long. The sample had no visible inclusions, even under high magnification. When cut, visible internal fractures along the **c**-axis were observed. These were avoided during both ERD and FTIR analyses.

HAM was originally ~17 mm in diameter and ~18 mm long. Small (≤1 mm diameter) brown and black inclusions were visible with the naked eye, and wafers were cut to avoid these inclusions. Similar to Cerro, visible internal fractures along the **c**-axis were observed after cutting, which were avoided during FTIR and ERD analyses.

Gem3 and Gem4 were from a batch of gem apatite crystals from an online vendor. Gem3 was originally ~7 mm in diameter and ~10 mm long. Microfractures were apparent in polished wafers, which may have resulted from either the cutting or polishing processes. Gem4 was originally ~6 mm in diameter and ~8 mm long. Internal cracks and large (~1 mm long) inclusions were apparent to the naked eye. Inclusions were polished away so that surfaces were flat for both ERD and FTIR analyses.

All samples were mounted on glass with Crystalbond for cutting and polishing. Samples were then cleaned with acetone and ethanol, and placed in a vacuum desiccator before analysis.

ERD analyses

All ERD analyses were carried out at the Michigan Ion Beam Laboratory at the University of Michigan with the 1.7 MV Tandetron accelerator. The instrument setup is similar to that discussed by Aubaud et al. (2009) and Bureau et al. (2009). In an ERD analysis, a beam of high-energy ions strikes the sample and knocks off H ions. Some recoiled H ions will escape from the incident surface to be recorded by detectors. In this study a 2 MeV He^{++} ion beam was

used. This energy allows us to analyze the hydrogen content in the sample to a depth of ~400 nm. Two detectors simultaneously collect the ERD and RBS (Rutherford back-scattering) spectra. The RBS spectrum is used to measure the number of particles incident on the sample during the acquisition of the ERD spectrum. An 8 μm Mylar® film was used in front of the ERD detector to filter out ions heavier than hydrogen and a Kapton ($H_{10}C_{22}N_2O_5$) foil was used as the hydrogen standard to determine the ERD detector solid angle ($\Delta\Omega$) (Wang 2004). No additional calibration or standards are needed to determine absolute hydrogen concentration using the ERD method (Tirira 1991; Aubaud et al. 2009; Bureau et al. 2009).

Apatite wafers were polished with SiC sandpaper and 0.3 μm alumina powder on cloth. The Cerro sample was coated with a Ni film a few nanometers thick to prevent charge build up during ion beam analysis because it was observed to spark during initial trials of ERD analysis. No other samples required such coating.

Atomic hydrogen concentration was determined through ERD and RBS spectrum modeling using the SIMNRA program (Mayer 1999). Some samples were run multiple times, with separate runs being modeled independently.

FTIR spectroscopy

Polarized IR spectra were acquired with a Perkin-Elmer Spectrum GX FTIR spectrometer using the microscope attachment, purged with N_2 gas. Instrument parameters for most runs were as follows: infrared source, KBr beamsplitter, KRS-5 IR wire grid polarizer for microscope, liquid nitrogen cooled MCT detector, 1 cm^{-1} resolution, IR range of 7800-400 cm^{-1}, and 50 μm x 50 μm aperture. Levitt and Condrate Sr. (1970) showed that the OH stretch band in apatite is not excited when the light vector **E** is perpendicular to the crystallographic **c**-axis, and maximum absorption occurs when **E** is parallel to **c**. Hence, samples were oriented and measured in

polarized, transmitted light, following the procedure of Levitt and Condrate Sr. (1970). In some cases, very small samples were placed on a KBr disc for analysis.

Apatite sections were cut parallel to the **c**-axis with a diamond wafering saw, and doubly polished with SiC sandpaper and 0.3 μm alumina powder on cloth. Because the OH absorbance band can be intense, samples were thinned down until absorbance over sample thickness was found to be constant after subsequent thinning. For our FTIR microscope setup, this has been observed to occur when peak heights are lower than ~1.3 absorbance units. As H_2O concentration increases, the required thickness decreases. The thinnest wafer in this study has a thickness of about 14 μ m. Some sample thicknesses (especially the thin samples) were determined using interference fringes between 3400-2100 cm^{-1}. Since values for index of refraction may vary with composition, n = 1.65±0.02 was used. Thicknesses determined from interference fringes were compared with directly measured thicknesses using a Mitutoyo digital micrometer (with an uncertainty of ±2 μm), and were in agreement within error, justifying the use of refractive index values for visible light wavelengths in the absence of refractive indices at 3400-2100 cm^{-1}. For samples where interference fringes were not present or not clean, thicknesses were measured on multiple spots using the micrometer.

Maximum linear absorbance peak height of the 3540 cm^{-1} band (OH stretch) and integrated absorbance area between 3670-3300 cm^{-1} were determined with the Spectrum program. Absorbance values were corrected against a linear baseline in all cases.

RESULTS

ERD analyses

Figure 1 shows selected ERD spectra for each sample. Actual counts are shown on the right vertical axis, and normalized counts by the number of incident ions are shown on the left

vertical axis. With the normalized counts, the "plateau" height is proportional to relative H concentration. Channel number denotes energy of the hydrogen ions detected by the ERD detector; higher channel number corresponds to higher energy. The energy of the detected hydrogen ion is related to the original depth of the hydrogen atom in the sample. Hydrogen ions from the surface of the samples have the highest energy. Therefore, channel number is also a proxy for shallowness; depth increases with decreasing channel number. The large peak at high channel numbers dominating each spectrum is the surface peak, commonly seen in ERD spectra (e.g., Bureau et al. 2009). This feature is attributed to adsorbed H. H concentration is determined by modeling the inner "plateau" height (between channel numbers 50 and 150). Note that even though we refer to it as a plateau for simplicity, there is a small slope to it (as can be seen from the data and model curve) at constant concentration due to energy straggling of the H ions as they pass through the sample and Mylar film. This effect can be modeled by the SIMNRA program. Table 1 lists all modeled atomic percents (at%) of H, as well as the corresponding calculated wt% H_2O. Original and modeled digital ERD spectra can be found in Supplementary Data.

Errors in the ERD method are discussed in Aubaud et al. (2009) and Bureau et al. (2009). The largest uncertainty comes from the statistical count rate. With $\leq$ 10 counts per channel and ~100 channels within the inner plateau, errors can reach 5-10%. There are also uncertainties involved when using the SIMNRA program to model the H concentration. Hence, the total uncertainty is larger than that based on counting statistics. For four of the five samples, multiple ERD measurements were made. The reproducibility error is often larger than the calculated error based on counting statistics. The reproducibility of multiple measurements is a better measure of the error and hence is used as the uncertainty for the calibration.

FTIR spectroscopy

All five samples showed maximum peak height at the same wavenumber (3540 cm^{-1}) and a single dominant peak (Figure 2). Table 2 summarizes the absorbance data. Both linear peak height and integrated peak area between 3670-3300 cm^{-1} were used for absorbance values in this calibration. The calibration using linear peak heights are for the convenience of users to rapidly estimate H_2O content in apatite. Because when **E**⊥**c**, the absorbance (either linear or integrated) cannot be resolved from the noise and is essentially zero, the measured absorbance at **E**//**c** is also the total absorbance summed along three eigen-directions.

An apatite crystal from Silver Crater Mine was also analyzed. The crystal was not gem-quality and was gray in color. Although the sample was transparent at its polished thickness of < 20 μm, numerous inclusions and imperfections were still apparent. The sample was analyzed using both ERD and FTIR. ERD showed 1.24 at% H (0.465 wt% H_2O), but FTIR measurements on several points avoiding inclusions and imperfections showed a very small OH peak, partially hidden within noise, which would correspond to ~0.04 wt% H_2O using our calibration. The inconsistency is attributed to inhomogeneity of the crystal and presence of small inclusions. Hence, this sample was not used in the calibration.

Due to the anisotropic properties of apatite, the accurate orientation of crystals during FTIR analysis is essential. Additional FTIR analysis was done on HAM, changing the polarizer in ten degree increments (Figure 3a). The data show that with the **E**-vector perpendicular to the **c**-axis, absorbance is 0 (Figure 3b). Figure 3 verifies the dependence of absorbance values on the angle between the **E**-vector and the crystallographic **c**-axis, which follow the formula given in Strens et al. (1982) and Libowitzky and Rossman (1996). Improper orientation of the polarizer relative to the crystal is thus an important factor in the error of IR absorbance values, since there

is a relatively steep absorbance difference with a small change in angle near the maximum. For our polarizer, each notch of the polarizer angle adjustment is 5˚, meaning the error is ≤ 2.5˚. This translates into a calculated relative error of 1% in the maximum peak height at **E**//**c**. Some polarizers may not be able to reproduce the zero absorbance for **E**⊥**c** due to inefficiency of the polarization. Original FTIR data, including spectra with **E**⊥**c** can be found in Supplementary Data.

Two other sources of error to consider in FTIR measurements are the choice of baseline when correcting spectra and the measurement of sample thickness. A linear baseline is used in all the absorbance values of this study. Typical uncertainty in A is ± 0.001 absorbance units. However, larger errors can occur when absorbance peak height is comparable to the amplitude of interference fringes. This can also complicate the interpretation of interference fringes when determining sample thickness.

During early FTIR analyses, it was observed that choice of aperture size had an effect on the absorbance band intensity. Notably, absorbances were lower when the aperture size was reduced from 300 μm x 300 μm to 100 μm x 100 μm. However, band intensities were within error for aperture sizes of 50 μm x 50 μm, 40 μm x 40 μm, and 30 μm x 30 μm. Therefore, to avoid additional error, we recommend only aperture sizes equal to or smaller than 50 μm x 50 μm when using this calibration.

Other peaks can also be seen in IR spectra. In particular, the CO_3^{2-} double peaks around 1500-1350 cm^{-1} (also at 870 cm^{-1}, though not shown; e.g., Fleet and Liu 2008) are observed to change with the angle of polarized light (Figure 4). The double peaks are the most uneven when the **E**-vector is parallel to the crystallographic **c**-axis, and approach similar peak heights when the **E**-vector is perpendicular to **c**.

Calibration

Plotting H_2O concentration against linear absorbance over sample thickness (Figure 5a) and using a modified York algorithm (York 1969) constrained to have an intercept of zero (personal communication, Chris Hall), we find that the weight percent of H_2O is 0.001199 ± 0.000029 times A/d, where d is the thickness in cm. The mean square weighted deviation (MSWD) is 0.8459, indicating a good fit since MSWD < 1. Using the molar mass of H_2O (18.015 g mol^{-1}) and the density of apatite (3.20 g cm^{-3}), the calculated molar absorptivity, ε = 470 ± 11 L mol^{-1} cm^{-1}. Using integrated absorbance, the weight percent of H_2O is (2.44 ± 0.06) $\times 10^{-5}$ times A/d with MSWD = 4.894 (Figure 5b). The reason for this less-than-satisfactory fit is not known. The corresponding molar absorptivity is $\varepsilon = (2.31 \pm 0.06) \times 10^4$ L mol^{-1} cm^{-2}.

DISCUSSION

There are now four different methods to analyze OH content in apatite: (i) electron microprobe and stoichiometry, (ii) IR, (iii) ERD, and (iv) SIMS. The electron microprobe analysis coupled with stoichiometry cannot provide accurate OH concentrations (see "Introduction"). The major advantages of the IR method lie in the ability to determine the hydrogen species (e.g., SIMS and ERD methods can detect total H, but cannot discern other species from OH), the ability to measure small samples, the precision and accuracy, and the low detection limit. Furthermore, FTIR is widely available, and the method is non-destructive in that after FTIR analysis, the sample may be analyzed using other methods. The main disadvantages are that the sample must be oriented and doubly polished.

For ERD, the main advantage is that it is an absolute method which does not require external calibration. The disadvantages include the (i) large sample size requirements, (ii) inability to distinguish among different forms of H, and (iii) high detection limit (> 100 ppm

H_2O).

The SIMS method uses a microbeam. The main advantages of SIMS are that it can measure small samples with adequate detection limit, there is no need to orient the sample, and only one side needs to be polished. The disadvantages are that it cannot distinguish different forms of H, and the detection limit is about 10 ppm (based on data in Boyce et al. 2010) rather than about 1 ppm for IR (see below). Furthermore, SIMS is not as widely available as FTIR.

Comparison of molar absorptivities with other minerals

For quantitative infrared analysis of anisotropic minerals, it is necessary to use total absorbance (summation of absorbances from polarized spectra in all three principal directions) (Libowitzky and Rossman 1996). Because absorbance is zero in the two principal directions when **E**⊥**c** for apatite (Figure 3), the absorbance we obtain at **E**//**c** is the total absorbance. For glasses and isotropic minerals such as garnet, the total absorbance is 3 times the absorbance along a given direction, and hence the molar absorptivity based on total absorbance is 3 times the molar absorptivity based on absorbance along any one direction.

Most minerals are calibrated for IR using integrated absorbance values. Aubaud et al. (2009) used ERD to determine molar absorptivities for olivine (ε = 34,515 L mol^{-1} cm^{-2}, where total absorbance by adding absorbances from 3 principal axes was used) and clinopyroxene (ε = 46,103 L mol^{-1} cm^{-2}). Bell et al. (1995) estimated the integrated molar absorptivity of garnet to be 3ε = 20,100 L mol^{-1} cm^{-2}. The apatite molar absorptivity from this study (ε = 23,100 L mol^{-1} cm^{-2}) is on the same order of magnitude. We can also compare our linear molar absorptivity for apatite (ε = 470 L mol^{-1} cm^{-1}) with that of rhyolitic glass based on total absorbance (3ε = 264 to 300 L mol^{-1} cm^{-1}; Newman et al 1986; Dobson et al. 1989; Aubaud et al. 2009), and we again find that they fall in the same order of magnitude.

Applications

With this calibration, it will be possible to utilize the IR method to obtain absolute water concentration for apatite crystals. Typical noise on a good IR spectrum is on the order of 0.001 linear absorbance units. Using our calibration, the detection limit of the IR method for a wafer of thickness 0.1 mm approaches ppm levels. Due to the ubiquitous presence of apatite in igneous and metamorphic rocks, and in terrestrial, lunar and martian rocks, and because it is important to know OH contents in apatite to constrain the formation conditions, our IR calibration may find widespread use. New data will provide better understanding of environments as close to home as terrestrial magma chambers and as far-ranging as lunar formation.

Furthermore, apatite may incorporate a variety of volatile components (H_2O, CO_2, SO_3, F, Cl). Combined with electron microprobe analyses to obtain major elements, and F and Cl concentrations (Stormer 1993; Henderson et al. 2010), as well as future development of FTIR for carbonate in apatite, apatite may become the most important mineral in studying volatile conditions of magma.

ACKNOWLEDGMENTS

We thank Eric Essene for his help in locating high-quality apatite crystals, Chris Hall for providing the modified York linear regression program for the case of zero intercept, and Artur Deditius and Bernard Evans for providing apatite samples and data. This research is supported by NASA (NNX10AH74G) and NSF (EAR-0838127 and EAR-1019440).

REFERENCES CITED

Aubaud, C., Bureau, H., Raepsaet, C., Khodja, H., Withers, A.C., Hirschmann, M.M., and Bell, D.R. (2009) Calibration of the infrared molar absorption coefficients for H in olivine, clinopyroxene and rhyolitic glass by elastic recoil detection analysis. Chemical Geology,

262, 78-86.

Bell, D.R., Ihinger, P.D., and Rossman, G.R. (1995) Quantitative-analysis of trace OH in garnet and pyroxenes. American Mineralogist, 80, 465-474.

Bhatnaga, V.M. (1967) Infra-red spectrum of an apatite from Wilberforce Ontario Canada. Archives of Oral Biology, 12, 429-430.

Boyce, J.W., and Hervig, R.L. (2009) Apatite as a monitor of late-stage magmatic processes at Volcan Irazú, Costa Rica. Contributions to Mineralogy and Petrology, 157, 135-145.

Boyce, J.W., Liu, Y., Rossman, G.R., Guan, Y.B., Eiler, J.M., Stolper, E.M., and Taylor, L.A. (2010) Lunar apatite with terrestrial volatile abundances. Nature, 466, 466-469.

Bureau, H., Raepsaet, C., Khodja, H., Carraro, A., and Aubaud, C. (2009) Determination of hydrogen content in geological samples using elastic recoil detection analysis (ERDA). Geochimica et Cosmochimica Acta, 73, 3311-3322.

Cherniak, D.J., Hervig, R., Koepke J., Zhang, Y., and Zhao, D. (2010) Analytical methods in diffusion studies. Reviews in Mineralogy and Geochemistry, 72, 107-170.

Dobson, P.F., Epstein, S., and Stolper, E.M. (1989) Hydrogen isotope fractionation between coexisting vapor and silicate-glasses and melts at low-pressure. Geochimica et Cosmochimica Acta, 53, 2723-2730.

Fleet, M.E., and Liu, X. (2008) Accommodation of the carbonate ion in fluorapatite synthesized at high pressure. American Mineralogist, 93, 1460-1469.

Henderson, C.E., Essene, E.J., Wang, K.L., and Zhang, Y. (2010) The perils of electron microprobe analysis of apatite. In: Eos 91 (AGU Fall Meeting), abstract V51C-2206.

Levitt, S.R., and Condrate, R.A., Sr. (1970) Polarized infrared spectra of hydroxyl ion in fluorapatite. Applied Spectroscopy, 24, 288-289.

Libowitzky, E., and Rossman, G.R. (1996) Principles of quantitative absorbance measurements in anisotropic crystals. Physics and Chemistry of Minerals, 23, 319-327.

Mathez, E.A., and Webster, J.D. (2005) Partitioning behavior of chlorine and fluorine in the system apatite-silicate melt-fluid. Geochimica et Cosmochimica Acta, 69, 1275-1286.

Mayer, M. (1999) SIMNRA, a simulation program for the analysis of NRA, RBS and ERDA. In: Duggan, J.L., and Morgan, I.L. (eds.) Application of Accelerators in Research and Industry, Pts 1 and 2, vol. 475, Aip Conference Proceedings, Melville, American Institute of Physics, pp. 541-544.

McCubbin, F.M., and Nekvasil, H. (2008) Maskelynite-hosted apatite in Chassigny meteorite: insights into late-stage magmatic volatile evolution in Martian magmas. American Mineralogist, 93, 676-684.

McCubbin, F.M., Steele, A., Nekvasil, H., Schnieders, A., Rose, T., Fries, M., Carpenter, P.K., and Jolliff, B.L. (2010) Detection of structurally bound hydroxyl in fluorapatite from Apollo Mare basalt 15058,128 using TOF-SIMS. American Mineralogist, 95, 1141-1150.

Nadeau, S.L., Epstein, S., and Stolper, E. (1999) Hydrogen and carbon abundances and isotopic ratios in apatite from alkaline intrusive complexes, with a focus on carbonatites. Geochimica et Cosmochimica Acta, 63, 1837-1851.

Newman, S., Stolper, E.M., and Epstein, S. (1986) Measurement of water in rhyolitic glasses – calibration of an infrared spectroscopic technique. American Mineralogist, 71, 1527-1541.

Stormer, J.C., Pierson, M.L., and Tacker, R.C. (1993) Variation of F-X-ray and Cl-X-ray intensity due to anisotropic diffusion in apatite during electron-microprobe analysis. American Mineralogist, 78, 641-648.

Strens, R.G.J., Mao, H.K., and Bell, P.M. (1982) Quantitative spectra and optics of some meteoritic and terrestrial titanian clinopyroxenes. In: Saxena, S.K. (ed.) Advances in physical geochemistry, vol. 2, Springer, New York, Heidelberg, Berlin, pp. 327-346.

Tacker, R.C. (2004) Hydroxyl ordering in igneous apatite. American Mineralogist, 89, 1411-1421.

Tirira, J., Frontier, J.P., Trocellier, P., and Trouslard, P. (1991) Development of a simulation algorithm for energy spectra of elastic recoil spectrometry. Nuclear Instruments and Methods in Physics Research, B54, 328-333.

Wang, Y.Q. (2004) Hydrogen standards in elastic recoil detection analysis. Nuclear Insruments and Methods in Physics Research B, 219-220, 115-124.

Webster, J.D., Tappen, C.M., and Mandeville, C.W. (2009) Partitioning behavior of chlorine and fluorine in the system apatite-melt-fluid. II: Felsic silicate systems at 200 MPa. Geochimica et Cosmochimica Acta, 73, 559-581.

York, D. (1969) Least-squares fitting of a straight line with correlated errors. Earth and Planetary Science Letters, 5, 320-324.

Table 1. ERD data for H atomic% and corresponding wt% H_2O in 5 apatite crystals

	DurMex	Cerro	HAM	Gem3	Gem4
H (atomic%)	0.23±0.01	0.21±0.01	1.13±0.03	1.3±0.1	1.15±0.07
		0.25±0.01	1.15±0.05	1.6±0.1	1.20±0.05
			1.17±0.02	1.7±0.1	1.25±0.04
			1.20±0.06		1.59±0.03
H_2O (wt%)	0.086±0.003	0.075±0.004	0.430±0.012	0.495±0.019	0.435±0.026
		0.095±0.003	0.435±0.017	0.607±0.022	0.455±0.019
			0.440±0.008	0.644±0.046	0.480±0.015
			0.455±0.023		0.607±0.012
Ave H_2O (wt%)	**0.086±0.003**	**0.085±0.014**	**0.440±0.011**	**0.582±0.078**	**0.494±0.077**

(1) Each entry represents a repeated measurement.

(2) Errors in at% H represent counting statistics, with relative error calculated as $1/\sqrt{n}$.

(3) Average H_2O in wt% is based on simple reproducibility (not weighted average) for samples that were measured multiple times.

Table 2. FTIR measurements

	DurMex	Cerro	HAM	Gem3	Gem4
d (μm)	59±2	59.8 57.3 61.1 61.1 58.7	32.5; 32.6; 32.9; 31.9; 32.3; 32.3; 32.0; 32.8; 33.2	16.9; 19.7; 21.6; 23.8; 16.0; 21.2	27.0; 14.2; 13.3; 13.6; 13.3; 12.8
A_{Lin}	0.414±0.027	0.541 0.520 0.550 0.547 0.528	1.191; 1.190; 1.219; 1.192; 1.188; 1.157; 1.092; 1.109; 1.101	0.833; 0.922; 1.016; 1.046; 0.786; 0.966	1.067; 0.667; 0.597; 0.616; 0.633; 0.601
Ave A_{Lin}/d (d in cm)	**70.1±5.2**	**90.1±0.5**	**357±16**	**470±20**	**451±30**
A_{Int}	13.9±1.8	23.0 22.8 23.6 23.5 22.9	63.2; 61.8; 62.6; 61.8; 63.5; 62.6; 59.4; 62.1; 60.5	33.9; 32.8; 37.3; 38.4; 24.7; 38.4	39.6; 19.8; 20.0; 26.0; 20.6; 22.5
Ave A_{Int}/d (d in cm)	**2363±315**	**3888±55**	**19067±471**	**17286±1663**	**15935±1961**

(1) A_{Lin} means linear absorbance. A_{Int} means integrated absorbance (area). Errors are given at 1s level.

(2) For DurMex, the error in A represent deviation of repeated IR measurements, the error in thickness is due to the digital micrometer (interference fringes are not clear for this sample); and the error in A/d is based on error propagation.

(3) For Cerro, Ham, Gem3, and Gem4, errors in A/d are based on multiple IR measurements with both thickness (from interference fringes) and absorbance from IR spectra.

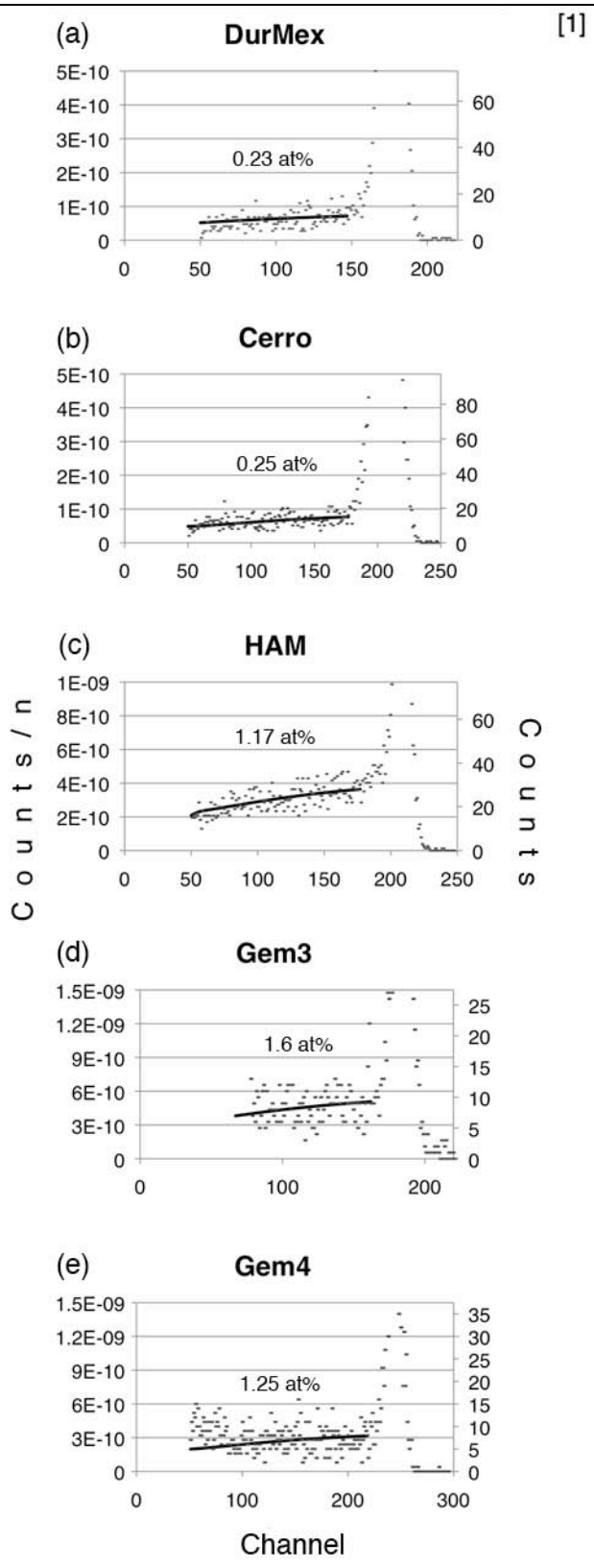

Figure 1. Selected ERD spectra with modeled fit plotting counts normalized by number of incident ions, and raw counts, against channel number (a proxy for shallowness into sample) for samples from **(a-b)** Durango, Mexico; **(c)** High Atlas Mountains, Morocco; **(d-e)** unknown locality, from an online vendor. The strong peak at high channel numbers is the surface peak, attributed to adsorbed H. Corresponding at% H values are obtained using the SIMNRA program.

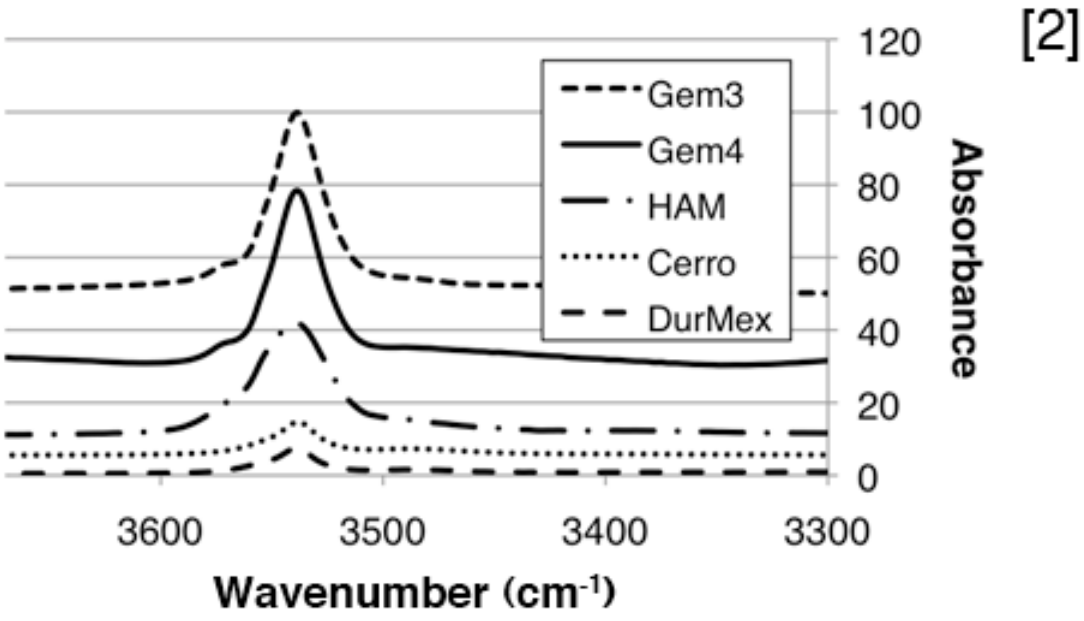

Figure 2. Selected IR spectra for each of the five samples of the OH stretch absorbance band when the light vector **E** is parallel to the crystallographic **c**-axis. Data has been normalized to 1 mm thickness and offset for comparison.

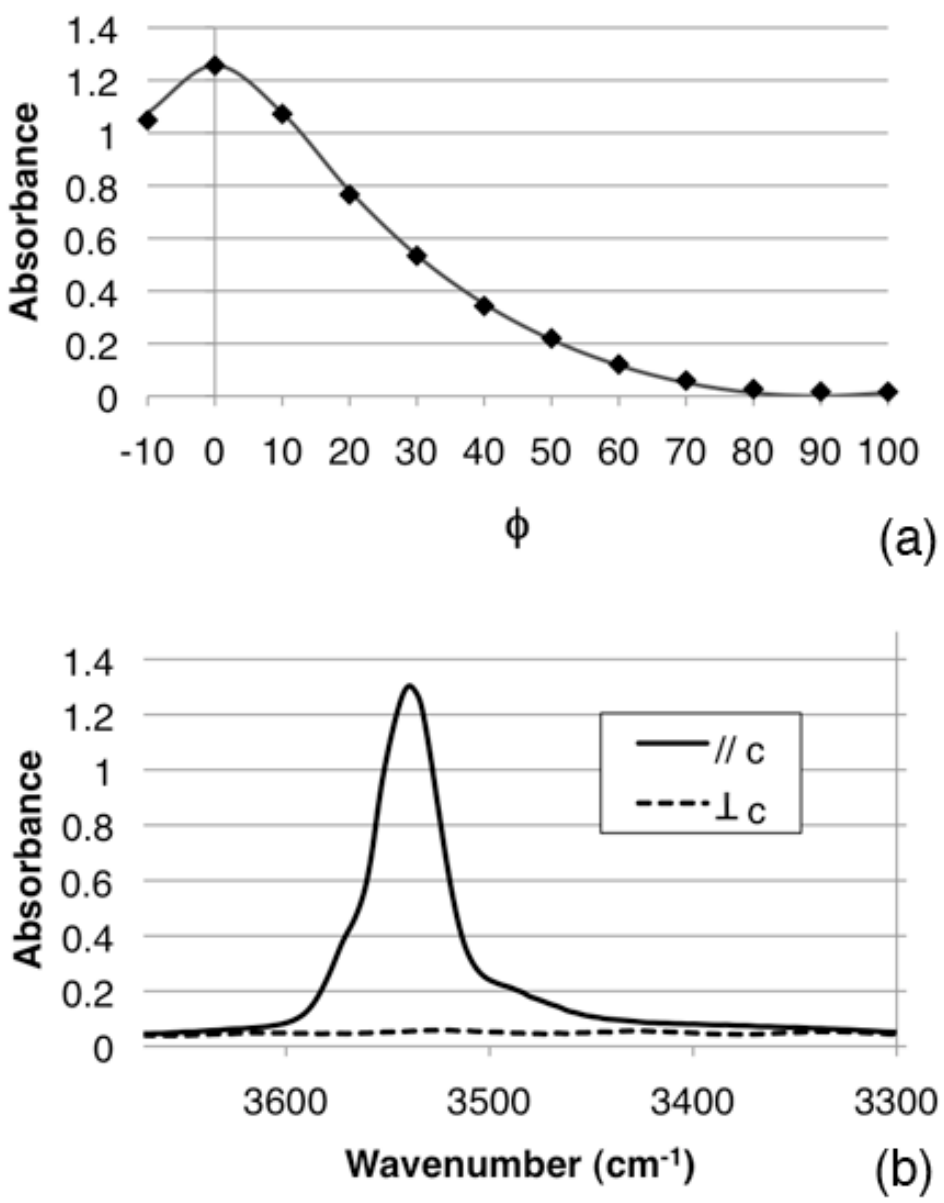

Figure 3. (a) Variation in absorbance due to angular alignment of polarized light with the crystallographic **c**-axis. Diamonds show measured absorbance peak heights from HAM, solid line is the calculated theoretical absorbance value following: $A(\phi) = -\log (10^{-A\max} \cos^2 \phi + 10^{-A\min} \sin^2 \phi)$, where ϕ is the angle between the **E**-vector and the **c**-axis. **(b)** FTIR spectra for HAM of the OH stretch absorbance band for **E**//**c** and **E**⊥**c**, showing that absorbance is 0 when **E** is perpendicular to the **c**-axis.

[4]

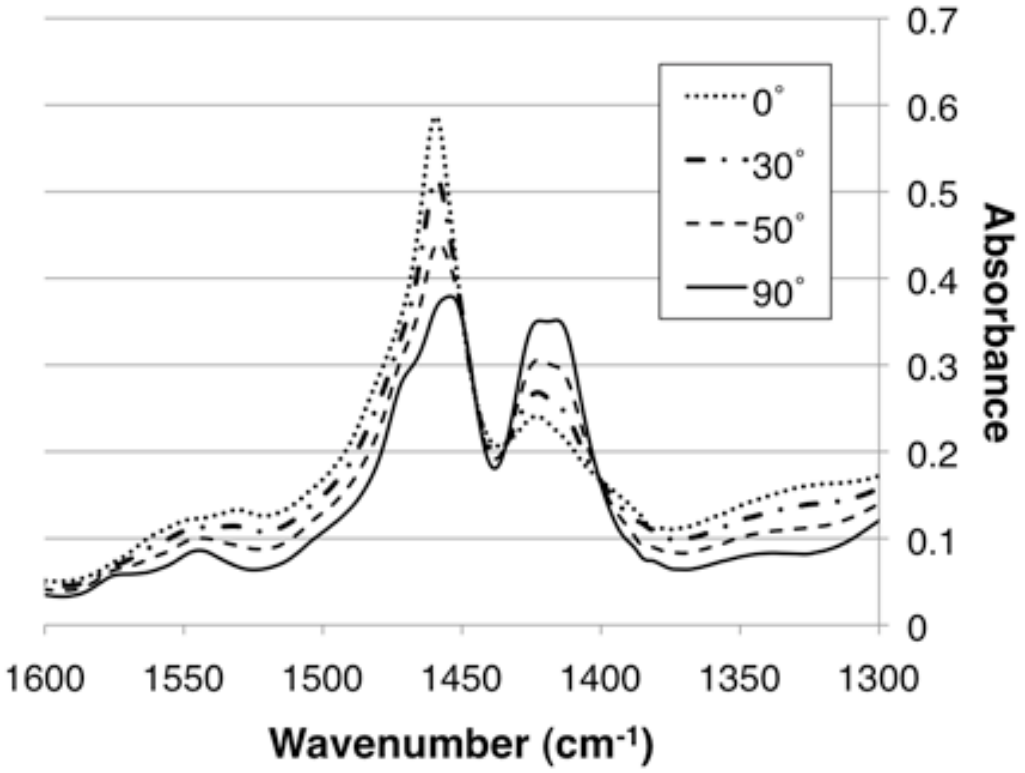

Figure 4. Variation in CO_3^{2-} absorbance in HAM sample due to angular alignment of polarized light with the crystallographic **c**-axis (angle denotes change from **c**-axis direction). The two bands approach similar peak heights when **E** is perpendicular to the **c**-axis.

[5]

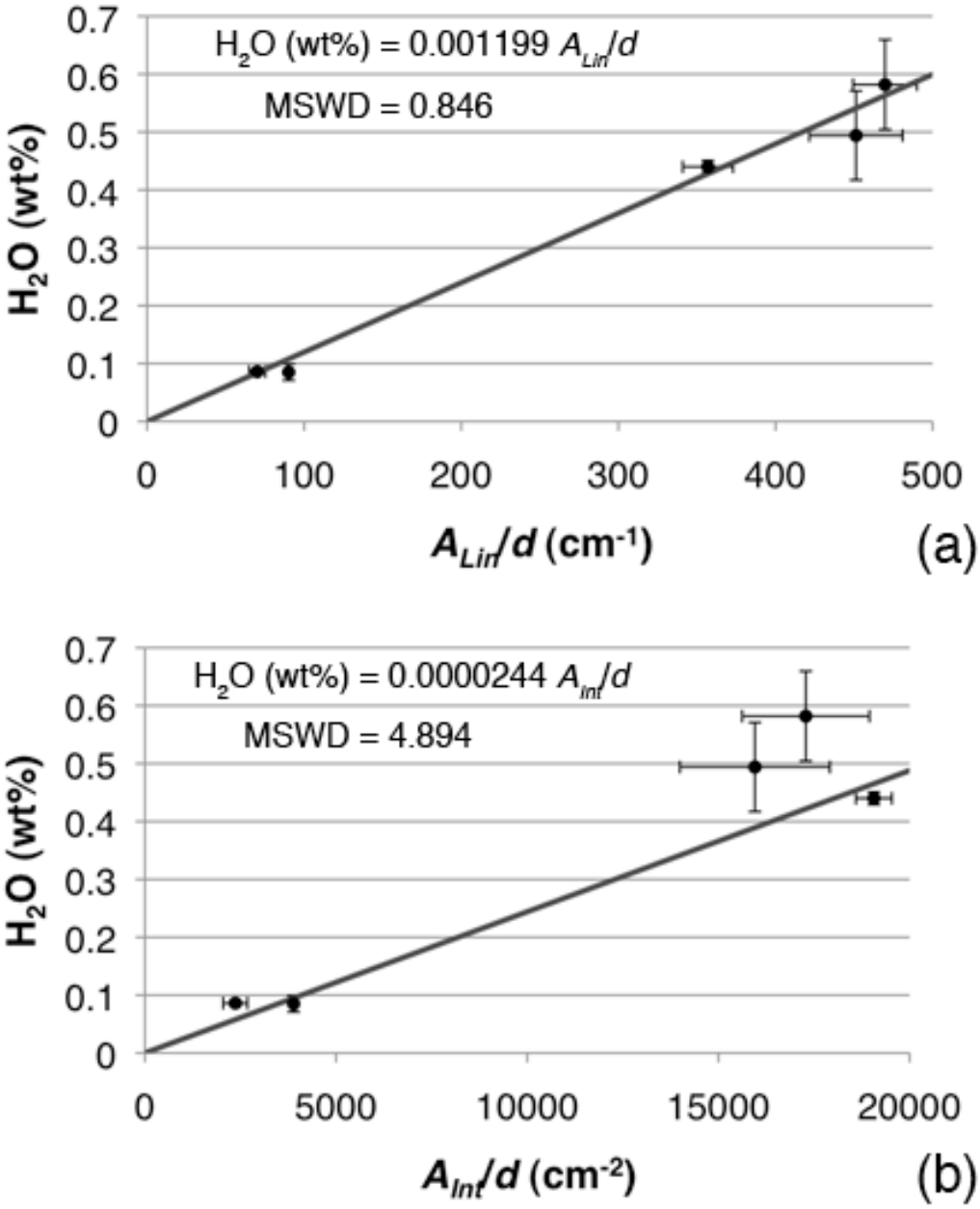

Figure 5. Calibration line for IR measurements of OH in apatite, where **(a)** A_{Lin} is linear absorbance peak height ~3540 cm^{-1} **(b)** A_{Int} is integrated absorbance between 3670-3300 cm^{-1}. Average wt% H_2O values are plotted on the vertical axis. Error bars are shown at 1σ level.